Early stages of magnetization relaxation in superconductors

Mihajlo Vanević,[1] Zoran Radović,[1] and Vladimir G. Kogan[2]

[1]*Department of Physics, University of Belgrade, Studentski Trg 12, 11158 Belgrade, Serbia*
[2]*Ames Laboratory DOE, Ames, Iowa 50011, USA*
(Received 18 February 2013; published 1 April 2013)

Magnetic flux dynamics in type-II superconductors is studied within the model of a viscous nonlinear diffusion of vortices for various sample geometries. We find that time dependence of magnetic moment relaxation after the field is switched off can be accurately approximated by $m(t) \propto 1 - \sqrt{t/\tilde{\tau}}$ in the narrow initial time interval and by $m(t) \propto (1 + t/\tau)^{-1}$ at later times before the flux creep sets in. The characteristic times $\tilde{\tau}$ and τ are proportional to the viscous drag coefficient η. Quantitative agreement with available experimental data is obtained for both conventional and high-temperature superconductors with η exceeding by many orders of magnitude the Bardeen-Stephen coefficient for free vortices. Huge enhancement of the drag, as well as its exponential temperature dependence, indicates a strong influence of pinning centers on the flux diffusion. Notwithstanding the complexity of the vortex motion in the presence of pinning and thermal agitation, we argue that the initial relaxation of magnetization can still be considered as a viscous flux flow with an effective drag coefficient.

Magnetic flux penetrates a type-II superconductor in the form of discrete quantized vortices. Vortex structures in conventional and high-temperature superconductors display remarkable complexity both in equilibrium[1,2] and dynamic regimes.[3–12] Relaxation of the magnetic moment of superconductors is achieved through initial viscous flux flow[13–18] and slow, logarithmic in time, thermally activated creep.[19–23] Thermally assisted hopping of vortices and vortex bundles between local minima in the random pinning potential is characteristic of both the creep and the flux flow under a driving force. In the latter, the hopping gives rise to the viscous drag coefficient $\eta \propto e^{U/kT}$, where U is the effective activation energy and T is the temperature.[21] A free flux flow regime can be realized at microwave frequencies (10–100 GHz) when the effect of the pinning is negligible. Measurements of surface impedance give viscous drag coefficients $\eta_0 \sim 10^{-6}$–10^{-7} Ns/m^2 at low temperatures for all superconductors, e.g., conventional NbSe$_2$ (Ref. 24), cuprates YBCO and BSCO,[25,26] and pnictide LiFeAs.[10] The order of magnitude is in accordance with the Bardeen-Stephen result for the viscous drag, $\eta_0 = \Phi_0 H_{c2}/\rho_n c^2$, caused by dissipation in the vortex core ($\Phi_0 = hc/2e$ is the flux quantum, ρ_n is the normal-state resistivity, and H_{c2} is the upper critical field).[4]

In this paper we study early stages of the flux dynamics after switching off the external magnetic field. We use a simple hydrodynamic approach: The local force the vortex experiences due to interaction with other vortices, the surface, and the local quenched disorder (pinning centers) is described by an effective viscosity $\eta \gg \eta_0$. The same approach successfully describes the vortex creep if supplemented by a phenomenological model of current-dependent or time-dependent activation energy, $U = U_c \ln(j_c/j)$ or $U = kT \ln(t/t_0)$, where j_c is the critical current and t_0 is the characteristic time scale for flux creep.[19–23]

We consider a model of massless vortex motion where the driving Lorentz force equals the viscous drag $(1/c)\mathbf{J} \times \boldsymbol{\Phi}_0 - \eta\mathbf{v} = 0$. Here, $\mathbf{J}$ is the current density, $\mathbf{v}$ is the vortex velocity, and η is a viscous drag coefficient. For magnetic induction $\mathbf{B} = n\boldsymbol{\Phi}_0$ related to the vortex density n, the force balance equation reads $(1/c)\mathbf{J} \times \mathbf{B} - \eta|B|\mathbf{v}/\Phi_0 = 0$, with

$\mathbf{J} = (c/4\pi)\nabla \times \mathbf{B}$. Taking into account the continuity equation $\partial B/\partial t + \nabla \cdot (B\mathbf{v}) = 0$, the dynamics of the magnetic flux in a superconductor is described by the well-known nonlinear diffusion equation[20–22]

$$\frac{\partial B}{\partial t} = \frac{\Phi_0}{4\pi\eta} \nabla \cdot (|B|\,\nabla B). \tag{1}$$

We have solved Eq. (1) for three sample geometries: a slab, a square-shaped plate, and a disk (see Fig. 1). We assume the sample thickness along the field is sufficiently large and neglect stray fields on the top and bottom of the sample. Magnetic induction $\mathbf{B}(\mathbf{r},t)$ is directed along the sample symmetry axis z and satisfies the following initial and boundary conditions: (i) B is uniform within the sample at $t = 0$, $B(x,y;t = 0) = B_0$, and (ii) B vanishes at the sample edges for $t > 0$.

For a long superconducting slab of width L, Eq. (1) reads

$$\frac{\partial B}{\partial t} = \frac{\Phi_0}{4\pi\eta} \frac{\partial}{\partial x}\left(|B|\,\frac{\partial B}{\partial x}\right), \tag{2}$$

where $B(x,t) = 0$ at $x = \pm L/2$ for $t > 0$. We can seek the solution in the form

$$B(x,t) = \sum_{k=1}^{\infty} B_k(t) \sin[k\pi(x/L + 1/2)], \tag{3}$$

with functions $B_k(t)$ to be determined from Eq. (2) and $B(x,t = 0) = B_0$. This gives the following set of differential
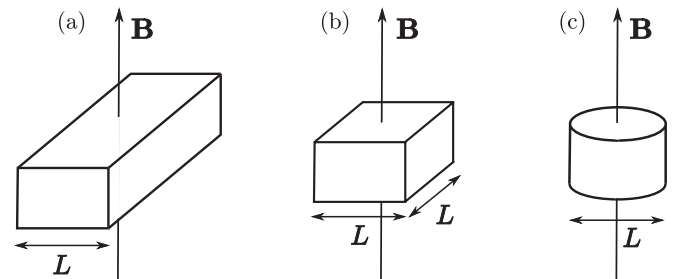

FIG. 1. Vortex dynamics is studied for three sample geometries: (a) a slab, (b) a square-shaped plate, and (c) a disk.
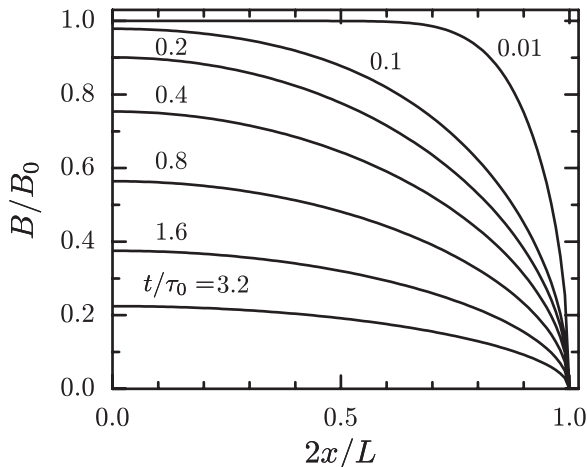
FIG. 2. Magnetic induction $B(x)$ across one half of a superconducting slab of width L is shown for times $t/\tau_0 = 0.01$, 0.1, 0.2, . . . ,3.2 (top to bottom).

equations:

$$\frac{dB_k(t)}{dt} = \frac{1}{B_0\tau_0} \sum_{i,j=1}^{\infty} B_i(t) F_k(i,j) B_j(t), \qquad (4)$$

with the initial conditions $B_k(0) = (2B_0/\pi k)[1 - (-1)^k]$ ($k = 1,2,\ldots$). Here, the coefficients $F_k(i,j)$ are given by

$$F_k(i,j) = \frac{k\pi}{4}\left(\frac{(i-j)^2}{(i-j)^2 - k^2} - \frac{(i+j)^2}{(i+j)^2 - k^2}\right) \qquad (5)$$

for $|i \pm j| \neq k$ and $i + j + k$ odd, and $F_k(i,j) = 0$ otherwise. The characteristic time constant is

$$\tau_0 = \frac{\pi L^2 \eta}{\Phi_0 B_0}. \qquad (6)$$

Equations (4) are solved by truncating the system at sufficiently large k ($k \sim 40$). The induction $B(x,t)$ for the slab is shown in Fig. 2 at various times $t/\tau_0 = 0.01$, 0.1, 0.2, . . . ,3.2. We observe that the flux flow near the sample edges in the initial time interval is very fast, reaching the center of the slab ($x = 0$) at time $t \sim 0.1\tau_0$ after switching off the field. This regime is followed by a slower flux flow taking place in the bulk of the sample.

The spatial dependence of the magnetic induction is in accordance with the previous results for the flux flow regime with constant activation energy.[22] In the presence of flux creep, which may take place in the center of the slab for $t \ll 0.1\tau_0$, or at large times $t \gg \tau_0$ when remanent magnetization is small, a phenomenological model of current and field-dependent activation energy should be used.[19–23] Note that the obtained $B(x,t)$ shown in Fig. 2 is qualitatively different from the solution of Eq. (2) when the field is switched on at $t = 0$. In that case the magnetic field enters the sample in the form of a flux front propagating from the edges.[20,22,27] Magnetic induction in the vicinity of the front is a linear function of the coordinate, $B(x,t) = (4\pi\eta/\Phi_0) v_f|x - x_f|$, with $x_f(t)$ and v_f being the position and the velocity of the front. In our case, the field is switched off at $t = 0$ and the flux escapes the sample with no front in $B(x,t)$ formed even at $t \ll \tau_0$. Indeed, at a sufficiently large distance u from the edge,
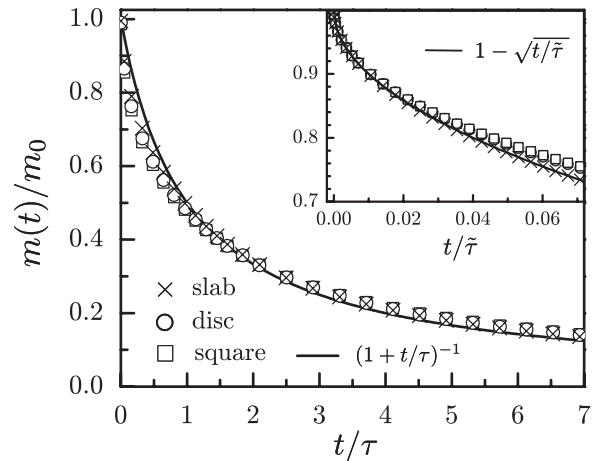

FIG. 3. Numerical solutions for magnetic moment relaxation for the slab ($\times$), disk ($\circ$), and square ($\square$) geometries, compared to the analytic approximation, Eq. (9) (solid line). Inset: A better fit for the initial time interval $t \ll \tau$ to the analytic expression, Eq. (7). In this case, only magnetization at the edges is affected by the flux flow.

Eq. (2) can be linearized with respect to $\delta B = B_0 - B$, which gives the exponential decay $\delta B(u,t) \propto (u/2\kappa\sqrt{t})^{-1} e^{-u^2/4\kappa^2 t}$ ($\kappa = \sqrt{\Phi_0 B_0/4\pi\eta}$) characteristic of the linear diffusion.

In the following we study the dynamics of the average magnetic induction $\bar{B}(t) = A^{-1}\int dx\,dy\, B(x,y,t)$ (A is the sample area) which is proportional to the magnetic moment $m(t)$ that can be measured. There are two regimes of the flux dynamics in the system. At very short times $t \ll \tau_0$ after switching off the field, the flux flow is localized near the edges and is unaffected by the sample size. In this case, the solution for a half-infinite superconductor is a good approximation, $B(u,t) = B_0 f(u/\kappa\sqrt{t})$ (Ref. 28). Here, f is a dimensionless function to be determined from Eq. (2) for the half-infinite superconductor with the boundary conditions $f(0) = 0$ and $f(\infty) = 1$. Using the above expression for $B(u,t)$ and taking into account that it deviates significantly from B_0 in the vicinity of the edges, we find for the average induction $1 - \bar{B}(t)/B_0 \propto (P/A)\kappa\sqrt{t}$, where P is the perimeter of the sample. This gives the magnetic moment relaxation

$$m(t) = m_0(1 - \sqrt{t/\tilde{\tau}}), \quad t \ll \tilde{\tau}, \qquad (7)$$

with the time constant

$$\tilde{\tau} = 9\pi(A/P)^2\eta/\Phi_0 B_0, \qquad (8)$$

where the numerical prefactor characterizes the spatial spread of B away from the edges. Comparison with the numerical solution for $m(t)$ is shown in the inset of Fig. 3 for different sample geometries. We find that Eq. (7) is a good approximation of the exact $m(t)$ in the short initial time interval $t/\tilde{\tau} \lesssim 0.1$ before the flux flow reaches the center of the sample. The flux flow in this time interval is very fast, leading to a 30% reduction of the overall magnetic moment.

At times $t \gtrsim \tau_0$ the flux flow extends through the whole sample, giving rise to the magnetization relaxation which depends on geometry. For the superconducting slab, the first-order approximation of Eq. (4) for $k = 1$ reads $\bar{B}^{(1)}(t) = (8B_0/\pi^2)[1 + t/(0.75\tau_0)]^{-1}$. Truncating Eq. (4) at
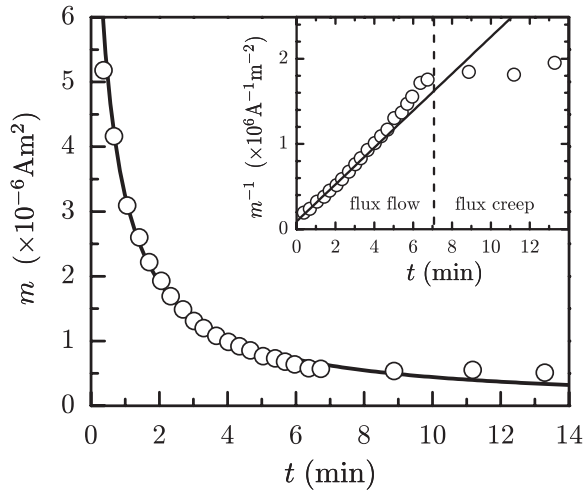
FIG. 4. Experimental data[14] ($\circ$) for the magnetic moment $m(t)$ in BSCO single crystal fitted to Eq. (9) with $m_0 = 1.1 \times 10^{-5}$ Am^2 and $\tau = 0.43$ min (solid curve). This corresponds to $\eta = 0.5$ Ns/m^2. Inset: The inverse magnetic moment as a function of time. The crossover between flux flow and flux creep regimes is seen as a dramatic change of the slope at $t \approx 7$ min (dashed line). The sample is a slab $0.14 \times 1.37 \times 2.06$ mm in size, the initial magnetic induction $B_0 = 35$ mT, and $T = 77$ K.

FIG. 5. Experimental data[15] ($\circ$) for magnetic moment relaxation in NbSe$_2$ monocrystal fitted to Eq. (7) (solid curve) with $\tilde{\tau} = 1.13 \times 10^3$ min, corresponding to $\eta = 11$ Ns/m^2. The dashed line indicates a crossover between the flux flow regime, Eq. (1), and the slow quasistatic motion before the flux creep. The sample has a square geometry $0.5 \times 0.5 \times 0.2$ mm, the initial magnetic induction $B_0 = 3.3$ mT, and $T = 4.2$ K.

$k \sim 40$, a practically exact solution is obtained. This solution can be approximated by a simple formula, $\bar{B}(t) = B_0[1 + t/(0.62\tau_0)]^{-1}$, which is very close to the exact one for $t \gtrsim \tau_0$. This suggests that the exact solution for the magnetic moment $m(t)$ can be accurately approximated by

$$m(t) = \frac{m_0}{1 + t/\tau}, \quad \tau = \alpha \tau_0, \tag{9}$$

where α is a number which depends on geometry. Fitting the exact numerical solution for $m(t)$ to Eq. (9) we find $\alpha = 0.620$, 0.244, and 0.226 for the slab, square, and disk geometries, respectively (Fig. 3). The fitting ensures the smallest absolute error between exact and fitted $m(t)$ for $1 < t/\tau < 3$. As expected, the decay of $m(t)$ is slower (that is, geometric factor α is larger) for the slab than for the disk, other parameters being equal.

In what follows, we analyze available experimental data on $m(t)$ and extract the characteristic time constant as well as the effective drag η. Relaxation of the magnetic moment in BSCO single crystals is studied in Ref. 14. Experimental data are shown in Fig. 4 (open circles) fitted to Eq. (9) (solid curve) with $m_0 = 1.1 \times 10^{-5}$ Am^2 and $\tau = 0.43$ min. The fitting is performed for the initial time interval before logarithmic in time, thermally activated flux creep sets in. The linear time dependence of the inverse magnetic moment is shown in the inset of Fig. 4; the crossover between flux flow and flux creep regimes is seen as a dramatic change of the slope at $t/\tau \approx 16$.

Let us now extract η. The dimensions of the sample used in the experiment are $0.14 \times 1.37 \times 2.06$ mm, which gives $B_0 = 4\pi m_0/V = 35$ mT, where V is the volume. Taking $\alpha = 0.620$ for the slab of the width $L = 0.14$ mm, we obtain $\eta = 0.5$ Ns/m^2. This value for the effective vortex viscosity exceeds by 6 orders of magnitude the Bardeen-Stephen drag
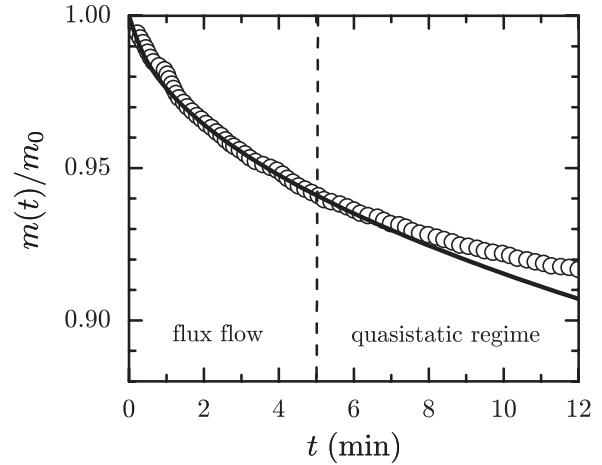
coefficient $\eta_0 \sim 10^{-7}$ Ns/m^2 measured in BSCO.[26] Huge enhancement of the drag indicates a strong influence of the pinning on the vortex diffusion. Despite the complexity of the vortex motion in the presence of pinning and thermal agitation, the magnetization follows a simple algebraic time dependence, Eq. (9).

Vortex dynamics has been studied in NbSe$_2$ using the decoration technique for visualization of flowing vortex lattices.[15] Magnetization measurements have been performed using the SQUID (superconducting quantum interference device) magnetometry. A crossover has been observed as a function of increasing flux density from a layered (smectic) flowing flux lattice in the disorder-dominated low-field limit to a more ordered (Bragg glass) lattice structure in the interaction-dominated high-field case. The observed time dependence of magnetization relaxation in the high-field limit ($B_0 = 3.3$ mT) is shown in Fig. 5. The regimes indicated in Fig. 5 correspond to the flux flow and to the quasistatic vortex motion. The solid curve in Fig. 5 is the fit of $m(t)$ to Eq. (7) for the NbSe$_2$ sample $0.5 \times 0.5 \times 0.2$ mm in size, which gives the relaxation time $\tilde{\tau} = 1.13 \times 10^3$ min and the viscous drag coefficient $\eta = 11$ Ns/m^2. We observe that the simple hydrodynamic model with an effective viscous drag force fits the data in the initial stages of magnetization relaxation where the vortex density is large and the flux flow takes place. The flux flow is localized near the edges, as corroborated experimentally by a small reduction of the magnetic moment of the sample over the measurement time and, more directly, by observing the static vortex structure in the center of the sample.[15] Large effective η is clearly due to hopping caused by successive pinning and thermally assisted depinning of vortices, as evidenced by studying single-vortex dynamics in pristine NbSe$_2$ monocrystals by scanning tunneling microscopy.[16]

Magnetic moment relaxations in YBCO polycrystal[17] and monocrystal[18] are shown in Figs. 6 and 7. The relaxation
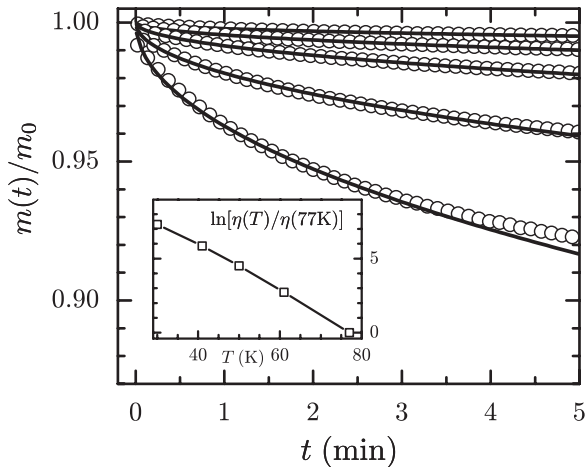
FIG. 6. Experimental data[17] (○) for magnetic moment relaxation in YBCO polycrystal at temperatures $T = 30$ K, 41 K, 50 K, 61 K, and 77 K (top to bottom), fitted to Eq. (7) (solid curves) with $\tilde{\tau} = 2.1 \times 10^5, 5.0 \times 10^4, 1.4 \times 10^4, 3.0 \times 10^3$, and 7.4×10^2 min, respectively. This corresponds to the drag coefficients $\eta = 284, 66, 17, 2.93$, and 0.19 Ns/m². Inset: Logarithm of the drag coefficient, normalized to $\eta(77 \text{K}) = 0.19$ Ns/m², as a function of the temperature. The sample has a rectangular geometry of $66 \times 34 \times 15$ mm. The initial magnetic induction is $B_0 = 3.95, 3.77, 3.48, 2.80, 0.735$ T, respectively.

FIG. 7. Experimental data[18] (○) for magnetic moment relaxation in YBCO monocrystal at temperatures of 85 K and 87 K (top to bottom), fitted to Eq. (7) with $\tilde{\tau} = 3.8 \times 10^3$ min and $\tilde{\tau} = 570$ min, respectively (solid curves). The corresponding drag coefficients are $\eta = 0.27$ and 0.04 Ns/m². The sample has a square geometry of $1 \times 1 \times 0.02$ mm, and the initial magnetic induction is $B_0 = 0.1$ mT.

in the polycrystalline YBCO (rectangular geometry, $66 \times 34 \times 15$ mm in size) is studied at 30 K, 41 K, 50 K, 61 K, and 77 K. The initial stage of magnetization relaxation can be fitted by Eq. (7) describing the flux flow in the vicinity of the edges (Fig. 6, solid curves). This is in agreement with the observed small reduction of the overall magnetic moment during the measurement. The obtained effective viscosity strongly depends on temperature, ranging between $\eta \sim 100$ and 0.1 Ns/m² as the temperature is increased from 30 K to 77 K, see inset of Fig. 6. The extracted value $\eta(77 \text{K}) = 0.19$ Ns/m² is consistent with the value $\eta = 0.12$ Ns/m² measured independently at the same temperature by studying the spatiotemporal change of the magnetization profile in a bulk YBCO sample in the flux-flow regime.[29] Taking $\eta \propto e^{U/kT}$ and neglecting the temperature dependence of the effective activation energy U as well as of the prefactor, we find $U \approx 360$ K in accordance with the previous results.[21]

Magnetic moment relaxation in small YBCO monocrystal ($1 \times 1 \times 0.02$ mm) is shown in Fig. 7.[18] The data can be fitted with the effective viscous drag coefficients $\eta = 0.27$ and 0.04 Ns/m² at temperatures of 85 K and 87 K, respectively. The decrease of η in such a narrow temperature range may be due to the proximity of the critical temperature ($T_c \approx 88$ K) where fluctuations are pronounced. In addition, the sharp change in the relaxation rate observed at 87 K and $t \approx 30$ min suggests that the flux flow is inhomogeneous and made of large domains which, upon depinning, abruptly increase the magnetic moment relaxation rate.

In conclusion, we have studied vortex dynamics in type-II superconductors in the initial time interval before the flux creep sets in. We have used a simple phenomenological (hydrodynamic) model of nonlinear diffusion of massless vortices where pinning of the flux lines by material
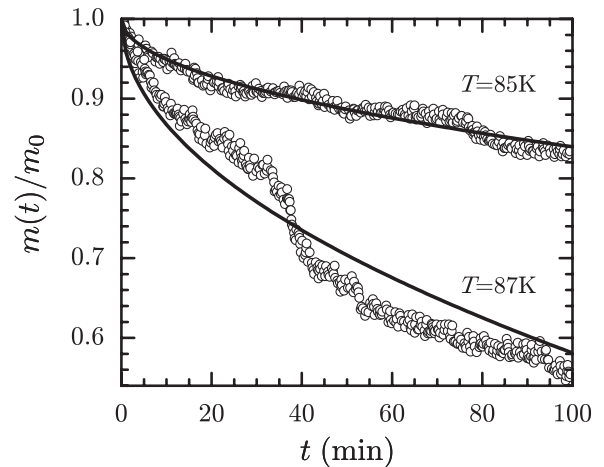
inhomogeneities, interaction with other vortices and the surface, and the Bardeen-Stephen dissipation in the vortex core are described by an effective viscous drag coefficient, η. After switching off the external magnetic field, the vortex dynamics exhibits two distinct regimes before the creep sets in with logarithmic in time decay of remanent magnetization. In the beginning, the flux flow is localized near the edges and is independent of the sample size. At later times, this regime is followed by a slower flux flow involving the bulk of the sample. We find that magnetic moment relaxation in these regimes can be accurately approximated by $m(t) = m_0(1 - \sqrt{t/\tilde{\tau}})$ for $t \ll \tilde{\tau}$ and $m(t) = m_0(1 + t/\tau)^{-1}$ for $t \gtrsim \tau$, where geometry-dependent $\tilde{\tau}$ and τ are proportional to η.

We have analyzed available experimental data on early stages of magnetization relaxation after the magnetic field is instantaneously removed. We obtained quantitative agreement for both conventional and high-temperature superconductors, albeit with η exceeding the Bardeen-Stephen value η_0 by many orders of magnitude. Huge enhancement of η with respect to η_0, as well as its exponential temperature dependence, indicates a strong influence of pinning and thermally assisted depinning of vortices on flux diffusion. We argue that early stages of magnetization relaxation can be modeled as a flux flow with an effective drag coefficient. This allows for a simple experimental determination of the bulk vortex viscosity, which cannot be accessed by the surface impedance measurements.

[1] G. W. Crabtree and D. R. Nelson, Phys. Today **50**, 38 (1997).

[2] E. H. Brandt, Rep. Prog. Phys. **58**, 1465 (1995).

[3] P. W. Anderson and Y. B. Kim, Rev. Mod. Phys. **36**, 39 (1964).

[4] J. Bardeen and M. J. Stephen, Phys. Rev. **140**, A1197 (1965).

[5] M. R. Beasley, R. Labusch, and W. W. Webb, Phys. Rev. **181**, 682 (1969).

[6] M. Tinkham, *Introduction to Superconductivity* (McGraw-Hill, New York, 1996).

[7] G. Blatter, M. V. Feigel'man, V. B. Geshkenbein, A. I. Larkin, and V. M. Vinokur, Rev. Mod. Phys. **66**, 1125 (1994).

[8] Y. Yeshurun, A. P. Malozemoff, and A. Shaulov, Rev. Mod. Phys. **68**, 911 (1996).

[9] M. C. Marchetti and D. R. Nelson, Phys. Rev. B **42**, 9938 (1990).

[10] T. Okada, H. Takahashi, Y. Imai, K. Kitagawa, K. Matsubayashi, Y. Uwatoko, and A. Maeda, Phys. Rev. B **86**, 064516 (2012).

[11] B. Raes, J. Van de Vondel, A. V. Silhanek, C. C. de Souza Silva, J. Gutierrez, R. B. G. Kramer, and V. V. Moshchalkov, Phys. Rev. B **86**, 064522 (2012).

[12] S.-Z. Lin, L. N. Bulaevskii, and C. D. Batista, Phys. Rev. B **86**, 180506 (2012).

[13] M. N. Kunchur, D. K. Christen, and J. M. Phillips, Phys. Rev. Lett. **70**, 998 (1993).

[14] V. Moshchalkov, A. Zhukov, V. Kuznetsov, V. Metlushko, and L. Leonyuk, JETP Lett. **50**, 91 (1989); Physica B (Amsterdam, Neth.) **169**, 609 (1991).

[15] F. Pardo, F. de la Cruz, P. L. Gammel, E. Bucher, and D. J. Bishop, Nature (London) **396**, 348 (1998).

[16] A. M. Troyanovski, J. Aarts, and P. H. Kes, Nature (London) **399**, 665 (1999).

[17] Z. Deng, K. Tsuzuki, M. Miki, B. Felder, S. Hara, and M. Izumi, J. Supercond. Novel Magn. **25**, 331 (2012).

[18] V. Y. Monarkha, V. P. Timofeev, and A. A. Shablo, Low Temp. Phys. **38**, 31 (2012).

[19] M. V. Feigel'man, V. B. Geshkenbein, A. I. Larkin, and V. M. Vinokur, Phys. Rev. Lett. **63**, 2303 (1989).

[20] V. M. Vinokur, M. V. Feigel'man, and V. B. Geshkenbein, Phys. Rev. Lett. **67**, 915 (1991).

[21] Y. Abulafia, A. Shaulov, Y. Wolfus, R. Prozorov, L. Burlachkov, Y. Yeshurun, D. Majer, E. Zeldov, and V. M. Vinokur, Phys. Rev. Lett. **75**, 2404 (1995).

[22] L. Burlachkov, D. Giller, and R. Prozorov, Phys. Rev. B **58**, 15067 (1998).

[23] A. Gurevich and H. Küpfer, Phys. Rev. B **48**, 6477 (1993).

[24] Y. S. Hor, U. Welp, Y. Ito, Z. L. Xiao, U. Patel, J. F. Mitchell, W. K. Kwok, and G. W. Crabtree, Appl. Phys. Lett. **87**, 142506 (2005).

[25] N. Pompeo and E. Silva, Phys. Rev. B **78**, 094503 (2008).

[26] M. Golosovsky, M. Tsindlekht, and D. Davidov, Supercond. Sci. Technol. **9**, 1 (1996).

[27] L. D. Landau and E. M. Lifshitz, *Fluid Mechanics*, Course of Theoretical Physics, Vol. 6 (Butterworth-Heinemann, 1987); F. Bass, B. Shapiro, I. Shapiro, and M. Shvartser, Physica C **297**, 269 (1998).

[28] V. V. Bryksin and S. N. Dorogovtsev, Sov. J. Exp. Theor. Phys. **77**, 791 (1993).

[29] S. I. Bondarenko, A. A. Shablo, and V. P. Koverya, Low Temp. Phys. **32**, 628 (2006).